

Egg-like magnetically immobilized nanospheres: A long-lived catalyst model for the hydrogen transfer reaction in a continuous-flow reactor

Yongjian Ai^{1,2}, Zenan Hu¹, Zixing Shao², Li Qi¹, Lei Liu¹, Junjie Zhou¹, Hongbin Sun¹ (✉), and Qionglin Liang² (✉)

¹ Department of Chemistry, Northeastern University, Shenyang 110819, China

² Department of Chemistry, Tsinghua University, Beijing 100084, China

Received: 27 January 2017

Revised: 27 March 2017

Accepted: 16 April 2017

© Tsinghua University Press
and Springer-Verlag GmbH
Germany 2017

KEYWORDS

magnetically immobilized,
continuous-flow,
egg-like,
catalytic reduction,
nitro compounds

ABSTRACT

A novel egg-like nanosphere was designed as a long-lived catalyst and is described as $\text{Fe}_3\text{O}_4@m\text{SiO}_2\text{-NH}_2\text{-Fe}_2\text{O}_3\cdot x\text{Bi}_2\text{O}_3@m\text{SiO}_2$. The catalyst was prepared using a modified Stöber method with template-free surface-protected etching. The catalyst particle consists of a magnetic Fe_3O_4 core as the “yolk”, an inner silica shell bearing active $\text{Fe}_2\text{O}_3\cdot x\text{Bi}_2\text{O}_3$ species as the “egg white”, and outer mesoporous silica as the “egg shell”. It exhibits an excellent performance in the catalytic reduction of nitro aromatics to corresponding anilines in a fixed-bed continuous-flow reactor. The reaction could be performed at 80 °C and could reach complete conversion in less than 1 min with only a 7% excess of hydrazine hydrate. The catalyst bed could be easily shifted between different substrates without cross-contamination because of the uniformity of the catalyst particles. This catalyst exhibited very good stability in the continuous-flow protocol. In the long-term reduction of *p*-nitrophenol with 0.5 mmol·min⁻¹ productivity, it worked for more than 1,500 cycles without any catalytic activity loss.

1 Introduction

Flow chemistry is a sophisticated and well-established enabling technique, and is widely used for industrial production of organic chemicals [1–4]. Many experiments can be handled with a continuous-flow microreactor, from milligram-level drug discovery to multigram-scale fine chemical preparation [5–6]. In these micro devices, reaction reagents are mixed so fast that the mass and heat transfer can be orders of

magnitude higher than that in classical batch reactors; thus, the risk of combustion and explosion is reduced [7–10]. Another obvious advantage of continuous-flow processing is that the heterogeneous catalyst can be straightforwardly immobilized into a fixed-bed reactor in the flow path [11–12]. The products are separated immediately from the heterogeneous catalyst, and the continuous manner provides an easy work-up procedure [13]. However, the heterogeneous catalysts are usually on the nanometer scale; these tiny particles

Address correspondence to Hongbin Sun, sunhb@mail.neu.edu.cn; Qionglin Liang, liangql@tsinghua.edu.cn

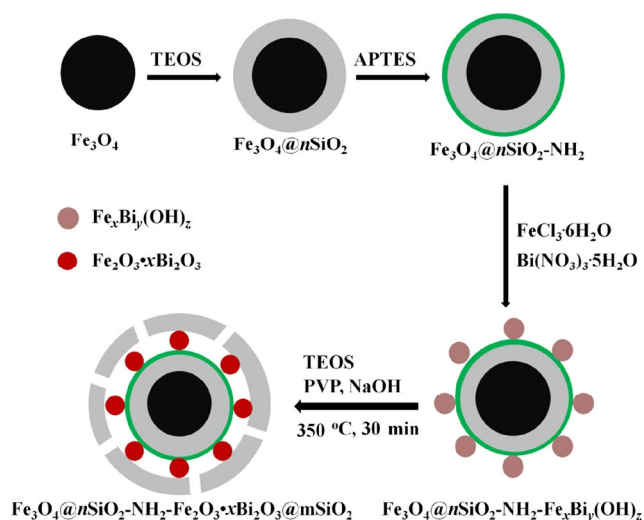
usually cause great pressure in the reaction tunnel, and they occasionally flow out from the catalyst bed with the reaction mixture and randomly block the reaction pipeline [14].

Loading the nanocatalyst onto a core–shell-structured mesoporous siliceous material is a reasonable solution for this issue [15–16]. Since their discovery in 1992, mesoporous siliceous core–shell-structured microspheres have been extensively applied in medicinal, biological, environmental, optical and chemical areas [17–22]. For several years, magnetic mesoporous silica-supported nanocatalysts have attracted particular attention [23–26]. The catalyst nanoparticles are encapsulated with mesoporous shells to make them stable, even under harsh reaction conditions, and chemical species can freely access the catalysts through the mesoporous shell of the nanocatalysts [27]. What's more, the catalysts are easily separable with an external magnetic field [28]. The importance of the core–shell catalysts has been verified by several papers [29–32]. Hence, we would like to report our newly developed magnetic nanosphere catalyst for the transformation of nitroarenes to anilines.

Anilines are key intermediates for the preparation of pharmaceuticals, agrochemicals, dyes, and antioxidants [33–34]. The total market value of arylamine will sharply increase to £10.17 billion by 2020 [35]. Anilines are generally obtained from the reduction of corresponding nitroarenes, and the highly efficient catalysts play a key role in this transformation [36]. Although catalytic hydrogenation is usually chosen for the reduction of nitroaromatics because H_2 is the cleanest hydrogen source, the selectivity is still a challenge, especially in the presence of other reducible groups [37]. Catalytic transfer hydrogenation (CTH) is convenient, and the catalytic reduction of nitroarenes is a trusted catalytic model for nanoparticles [38]. The catalytic H-transfer procedure was widely adopted with different hydrogen sources, such as sodium borohydride, silanes, boranes, formic acid, H_2 , and hydrazine hydrate [39]. Many chemoselective and highly efficient noble metal catalysts are used for catalytic reduction, including Au [40–43], Ru [44–45], Pt [46–48], Pd [49–52], and Rh [53–54], with various hydrogen sources. However, the high price of the noble metals limited their further applications in industry;

thus, non-noble metal catalysts, especially Fe-based catalysts, have aroused much interest in this transformation because of their low toxicity, low cost, and environmental friendliness [55–59]. Hydrazine is the most reactive hydrogen source for Fe-based catalysts, and it is a clean reactant because the only by-products are N_2 and water. The main problem for the Fe-based catalysts is that the nanoparticles usually tend to aggregate and then lose their original catalyst activity because of their high surface energy [60]. Thus, designing efficient Fe-based catalysts with more stable structures has increasingly attracted the attention of chemists and materials scientists.

The continuous reduction of nitroaromatics to corresponding anilines has been considered because it takes advantages of highly efficient, safe, and easy work-up procedures [58, 61–63]. We designed a novel structural catalyst based on magnetic silica spheres, and it exhibited a good activity and an ultra-long lifetime for continuous hydrazine-mediated reduction of nitro compounds. The developed catalyst is described as $Fe_3O_4@nSiO_2-NH_2-Fe_2O_3 \cdot xBi_2O_3@mSiO_2$, and it is an egg-like nanocatalyst. The inner core is a magnetic Fe_3O_4 sphere with an average diameter of 200 nm, and it is wrapped by a layer of nonporous silica. The amino group is introduced to the surface of the silica sphere. The Fe-based catalyst nanoparticles are magnetically immobilized around the magnetic silica spheres, and they are well dispersed and bound to the surface by the amino group. The catalyst layer is further encapsulated with another layer of silica, which can inhibit catalyst leaching and agglomeration. The whole catalyst nanosphere is protected by polyvinylpyrrolidone (PVP), and then etched with NaOH to enhance the permeability of the outer silica shell. The final catalyst was obtained after calcining at 350 °C to improve the robustness and thermally remove PVP (Scheme 1). The catalyst was applied in a catalyst cartridge that was connected in a continuous-flow reactor for the reduction of substituted nitroarenes. This egg-like nanocatalyst system showed an excellent catalytic performance, while the reactions were completed in 1 min at 80 °C with only 7% stoichiometric excess of hydrazine hydrate. The catalyst cartridge can be easily switched between different substrates because of the uniform catalyst particle size, and no residue is detectable in



Scheme 1 Synthesis of the magnetic $\text{Fe}_3\text{O}_4@n\text{SiO}_2\text{-NH}_2\text{-Fe}_2\text{O}_3 \cdot x\text{Bi}_2\text{O}_3@m\text{SiO}_2$ core-shell nanocatalyst.

the sequential product. Furthermore, the long-term catalyst test demonstrated that this heterogeneous catalyst system was sufficiently stable and its activity was maintained for more than 1 day for the reduction of *p*-nitrophenol. This protocol sets a model for the long-lived catalyst for CTH.

2 Experimental

2.1 Preparation of $\text{Fe}_3\text{O}_4@n\text{SiO}_2$

The $\text{Fe}_3\text{O}_4@n\text{SiO}_2$ core nanocomposite was prepared by a modified Stöber method, as previously reported [64]. The received Fe_3O_4 nanoparticles (100–300 nm) were first treated with dilute HCl because the magnetic ferrite was not very water-dispersible. Generally, 0.30 g of Fe_3O_4 was added to 60 mL of 0.1 M aqueous HCl and sonicated for 10 min. Then, the magnetite spheres were quickly collected by an external magnet and washed with deionized water until the pH of the solution became near-neutral (~7). Fe_3O_4 was then homogeneously dispersed in a blend of ethanol (200 mL), deionized water (40 mL), and concentrated aqueous ammonia (4 mL, 25 wt.%). After a 30 min ultrasound treatment, 0.5 mL of tetraethyl orthosilicate (TEOS) was slowly added to this suspension, and this mixture was stirred for 6 h at room temperature. Finally, the $\text{Fe}_3\text{O}_4@n\text{SiO}_2$ nanocomposite was separated using a magnet and washed with water and ethanol; the

separated residue was dried at 60 °C for 6 h and stored under vacuum for further use.

2.2 Preparation of $\text{Fe}_3\text{O}_4@n\text{SiO}_2\text{-NH}_2$

The -NH_2 -terminated $\text{Fe}_3\text{O}_4@n\text{SiO}_2$ colloids were synthesized as reported by Ge et al. [65]. The dried $\text{Fe}_3\text{O}_4@n\text{SiO}_2$ nanoparticles were transferred into an anhydrous mixed solution of isopropanol (200 mL) and 3-aminopropyl-triethoxysilane (0.5 mL). After the nanoparticles became highly dispersed, the mixture was heated at 80 °C for 3 h to functionalize the silica surface with amino groups. As the solution was cooled to room temperature, the $\text{Fe}_3\text{O}_4@n\text{SiO}_2\text{-NH}_2$ colloids were washed with isopropanol and deionized water, and then separated using a magnet. Eventually, the black $\text{Fe}_3\text{O}_4@n\text{SiO}_2\text{-NH}_2$ colloids were dispersed in 100 mL of deionized water.

2.3 Preparation of $\text{Fe}_3\text{O}_4@n\text{SiO}_2\text{-NH}_2\text{-Fe}_x\text{Bi}_y(\text{OH})_z$

The typical synthesis of $\text{Fe}_3\text{O}_4@n\text{SiO}_2\text{-NH}_2\text{-Fe}_x\text{Bi}_y(\text{OH})_z$ was performed as follows. Briefly, the homo-dispersed solution of $\text{Fe}_3\text{O}_4@n\text{SiO}_2\text{-NH}_2$ (100 mL) was loaded into a round-bottom flask. Another solution containing 100 mg of $\text{Bi}(\text{NO}_3)_3 \cdot 5\text{H}_2\text{O}$, 1.00 g of $\text{FeCl}_3 \cdot 6\text{H}_2\text{O}$, 75 mL of absolute ethanol, and 25 mL of deionized water, which had been sonicated for 1 h, was added to the $\text{Fe}_3\text{O}_4@n\text{SiO}_2\text{-NH}_2$ solution. The resulting mixture was stirred using a magnetic bar for 1 h at 90 °C. Then, a 28% concentrated ammonia solution was slowly added to increase the solution pH to 12. The resulting solution was rapidly stirred for another 6 h at 90 °C. After the iron and bismuth ions were sufficiently deposited, the resulting $\text{Fe}_3\text{O}_4@n\text{SiO}_2\text{-NH}_2\text{-Fe}_x\text{Bi}_y(\text{OH})_z$ nanoparticles were collected by filtration and washed with ethanol and deionized water.

2.4 Preparation of the $\text{Fe}_3\text{O}_4@n\text{SiO}_2\text{-NH}_2\text{-Fe}_2\text{O}_3 \cdot x\text{Bi}_2\text{O}_3@m\text{SiO}_2$ nanocatalyst

The SiO_2 shell was prepared using a slightly modified version of the method used to prepare the first layer. After the $\text{Fe}_3\text{O}_4@n\text{SiO}_2\text{-NH}_2\text{-Fe}_2\text{O}_3 \cdot x\text{Bi}_2\text{O}_3$ colloids were dispersed in a mixed solution of ethanol, deionized water, and concentrated aqueous ammonia (200 + 40 + 4 mL, respectively), 1.5 mL of TEOS was added; then, the mixture was stirred at room temperature overnight.

After filtration, the residue was dissolved in 50 mL of deionized water; then, a PVP sol (1.2 g PVP dissolved in 10 mL of deionized water) was added, and the mixture was refluxed at 100 °C for 3 h. The solution was naturally cooled to room temperature; then, 10 mL of a 0.16 g·mL⁻¹ NaOH solution was injected into the system to etch the surface of SiO₂. After etching for 60 min (the etching time dramatically influenced the catalyst activity, and we determined that the best activity was obtained with a 60 min etching time; more details are available in Fig. S1 in the Electronic Supplementary Material (ESM), Fe₃O₄@*n*SiO₂-NH₂-FeBiO_{*x*}@*m*SiO₂ was filtered and washed with large amounts of deionized water. The filter cake was dried at 80 °C overnight. Ultimately, it was calcined at 350 °C for 30 min in a muffle furnace to obtain about 650 mg of the magnetic Fe₃O₄@*n*SiO₂-NH₂-Fe₂O₃·*x*Bi₂O₃@*m*SiO₂ nanocatalyst.

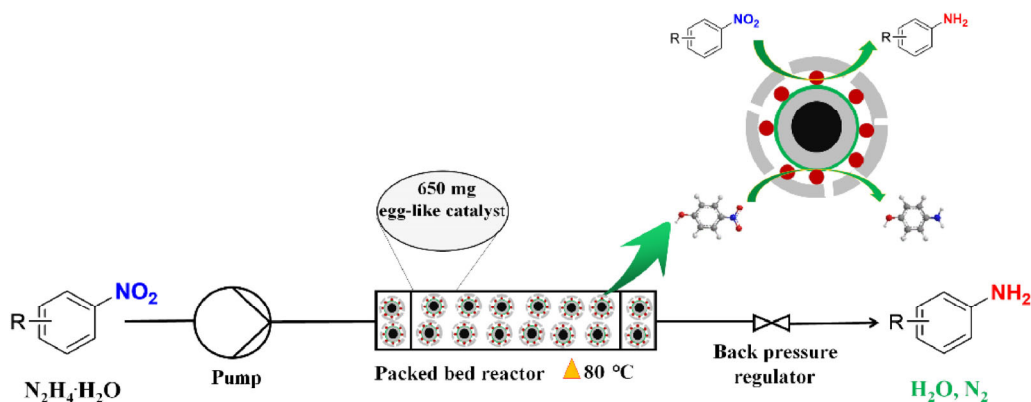
2.5 Catalyst activity test

The reduction of *p*-nitrophenol was performed in a self-made continuous-flow microreactor, which is illustrated in Scheme 2. To test the catalytic activity, 650 mg of the Fe₃O₄@*n*SiO₂-NH₂-Fe₂O₃·*x*Bi₂O₃@*m*SiO₂ nanocatalyst was mixed with 1,200 mg of silica gel to “dilute” the catalyst. Then, this mixture was placed in a 4.6 mm × 150 mm blank high performance liquid chromatography (HPLC) column to form the catalyst cartridge. The free volume in the microreactor was estimated as about 1.0 mL using the methanol filling method. After connecting to the continuous-flow reactor, the catalyst cartridge was heated at 80 °C in silicon

oil. A solution of 4-nitrophenol (5,560 mg, 40 mmol), hydrazine hydrate (4,000 mg, 64 mmol, 80%), and methanol (80 mL) was pumped through the heated catalyst bed by a HPLC pump at a flow rate of 1 mL·min⁻¹. The input yellow solution was rapidly converted to a colorless solution; this indicated that *p*-nitrophenol was entirely reduced to *p*-aminophenol. The reaction process was also monitored by HPLC and thin layer chromatography (TLC), and no byproducts were detected. The solvent was removed under a reduced pressure, and the obtained residual was diluted with water and extracted with ethyl acetate. The extractant was evaporated under reduced pressure and the products were purified by recrystallation from ethyl acetate. This continuous-flow processing was also applied for reducing varieties of aromatic compounds and long run reduction of *p*-nitrophenol to test the scope and stability of the catalyst. All of the products were characterized by ¹H nuclear magnetic resonance (NMR) spectroscopy, ¹³C NMR spectroscopy, and gas chromatography-mass spectrometry (GC-MS).

3 Results and discussion

We began our research by exploring the most active catalyst. If the active component, Fe₂O₃·*x*Bi₂O₃, was used directly without loading it on a supporter, its catalytic activity was poor and it could not be recovered. Noticing that the iron oxide-based active centers of Fe₂O₃·*x*Bi₂O₃ were magnetic, we immobilized them on the magnetic silica spheres. A series of egg-like catalysts were synthesized and examined for the



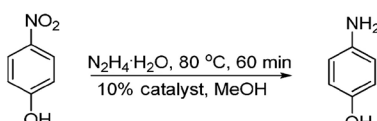
Scheme 2 Fixed-bed continuous-flow format for the reduction of nitroarenes with the Fe₃O₄@*n*SiO₂-NH₂-Fe₂O₃·*x*Bi₂O₃@*m*SiO₂ nanocatalyst.

reduction of *p*-nitrophenol in a sealed tube (Table 1), and we found that $\text{Fe}_2\text{O}_3 \cdot x\text{Bi}_2\text{O}_3$ was the most efficient active center of the tested catalysts. The amino group that was introduced on the inner silica layer further promoted catalytic activity. In the presence of the amino group that dispersed and stabilized the active metal oxide particles, the catalytic activity of SS-Fe-Bi showed perfect activity as the conversion of *p*-nitrophenol was >99% (entry 1), while the conversion of *p*-nitrophenol was only 80% over SS-nFe-Bi (entry 2), whose activity was less than the SS-Fe catalyst (entry 3). Considering the benefit of metal oxide modification, varieties of oxide-included $\text{Fe}_3\text{O}_4@n\text{SiO}_2\text{-NH}_2\text{-Fe}_2\text{O}_3 \cdot x\text{M}_y\text{O}_z@m\text{SiO}_2$ catalysts were prepared and evaluated with the reduction of *p*-nitrophenol. They were all less active than SS-Fe-Bi. In particular, the Mg-, Zn-, and Cu-containing catalysts (SS-Fe-Mg, SS-Fe-Zn, and SS-Fe-Cu) provided non-promising conversions (entries 4–6). To our relief, the Sb_2O_3 -, Al_2O_3 -, and NiO-modified catalysts (SS-Fe-Sb, SS-Fe-Al, and SS-Fe-Ni) were better than the pure iron oxide-based catalyst (SS-Fe) (entries 7–9 vs. entry 3, respectively). In particular, Sb, which is in the same column of the periodic table as

Bi, showed a superior activity to all of the other metals, except Bi, with a conversion of 95% (entry 4). We deduced that the Lewis acidic site in the composite oxide was the key point to enhance the catalytic activity. In the present report [66], the active H species that are generated from N_2H_4 on the surface of the metal oxide are in terms of $\text{H}^{\delta-}$, and the metal oxide can provide a Lewis acid site, such as Bi_2O_3 , Sb_2O_3 , or NiO, which may stabilize $\text{H}^{\delta-}$; thus, the oxide composites show better activities than the pure iron oxide.

The well-developed catalyst was characterized by high-resolution transmission electron microscopy (HRTEM), scanning transmission electron microscopy (STEM), energy dispersive X-ray spectroscopy (EDS), X-ray diffraction (XRD), X-ray photoelectron spectroscopy (XPS), and vibrating sample magnetometer (VSM). The transmission electron microscopy (TEM) result shows that SS-Fe-Bi was in an approximately spherical morphology with an average diameter of 300 nm (Figs. 1(a), 1(b), and S2–S4 in the ESM).

Table 1 Reduction of *p*-nitrophenol over a series of egg-like nanocatalysts^a



Entry	Catalyst	Conversion (%) ^b
1	$\text{Fe}_3\text{O}_4@n\text{SiO}_2\text{-NH}_2\text{-Fe}_2\text{O}_3 \cdot x\text{Bi}_2\text{O}_3@m\text{SiO}_2$	SS-Fe-Bi >99
2	$\text{Fe}_3\text{O}_4@n\text{SiO}_2\text{-Fe}_2\text{O}_3 \cdot x\text{Bi}_2\text{O}_3@m\text{SiO}_2$	SS-nFe-Bi 80
3	$\text{Fe}_3\text{O}_4@n\text{SiO}_2\text{-NH}_2\text{-Fe}_2\text{O}_3@m\text{SiO}_2$	SS-Fe 90
4	$\text{Fe}_3\text{O}_4@n\text{SiO}_2\text{-NH}_2\text{-Fe}_2\text{O}_3 \cdot x\text{MgO}@m\text{SiO}_2$	SS-Fe-Mg 30
5	$\text{Fe}_3\text{O}_4@n\text{SiO}_2\text{-NH}_2\text{-Fe}_2\text{O}_3 \cdot x\text{ZnO}@m\text{SiO}_2$	SS-Fe-Zn 26
6	$\text{Fe}_3\text{O}_4@n\text{SiO}_2\text{-NH}_2\text{-Fe}_2\text{O}_3 \cdot x\text{CuO}@m\text{SiO}_2$	SS-Fe-Cu 75
7	$\text{Fe}_3\text{O}_4@n\text{SiO}_2\text{-NH}_2\text{-Fe}_2\text{O}_3 \cdot x\text{Sb}_2\text{O}_3@m\text{SiO}_2$	SS-Fe-Sb 95
8	$\text{Fe}_3\text{O}_4@n\text{SiO}_2\text{-NH}_2\text{-Fe}_2\text{O}_3 \cdot x\text{Al}_2\text{O}_3@m\text{SiO}_2$	SS-Fe-Al 92
9	$\text{Fe}_3\text{O}_4@n\text{SiO}_2\text{-NH}_2\text{-Fe}_2\text{O}_3 \cdot x\text{NiO}@m\text{SiO}_2$	SS-Fe-Ni 93
10	$\text{Fe}_3\text{O}_4@n\text{SiO}_2\text{-NH}_2@m\text{SiO}_2$	SS 0

^aAll reactions were performed with 1 mmol of *p*-nitrophenol and 2.0 eq. of hydrazine hydrate in 2 mL of methanol, 10 mmol% catalyst.

^bDetermined as an HPLC peak area percentage.

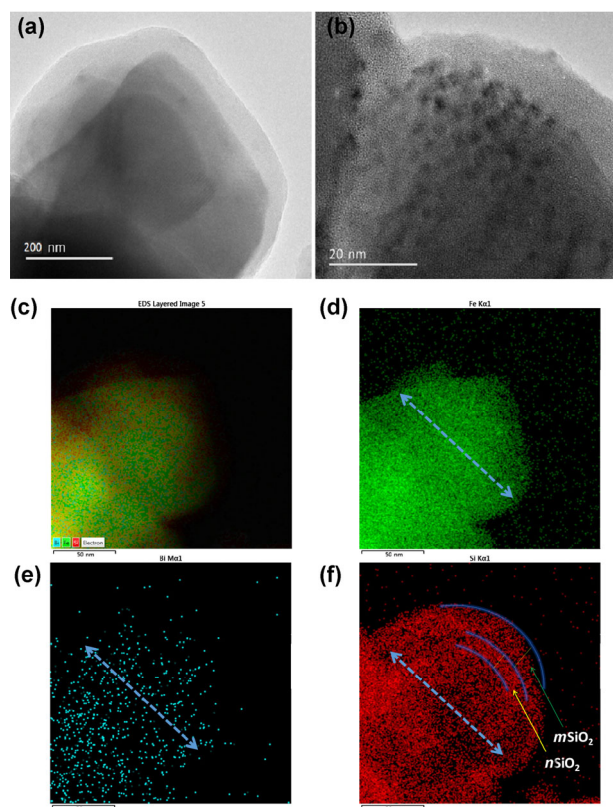


Figure 1 HRTEM images of (a) and (b) $\text{Fe}_3\text{O}_4@n\text{SiO}_2\text{-NH}_2\text{-Fe}_2\text{O}_3 \cdot x\text{Bi}_2\text{O}_3@m\text{SiO}_2$. EDS mapping of (c) $\text{Fe}_3\text{O}_4@n\text{SiO}_2\text{-NH}_2\text{-Fe}_2\text{O}_3 \cdot x\text{Bi}_2\text{O}_3@m\text{SiO}_2$ and individual (d) Fe, (e) Si, and (f) Bi nanoparticles (green: Fe, red: Si, blue: Bi).

The etched nanocomposite has a clear egg-like structure with Fe_3O_4 as the yolk, the inner nonporous silica loading with $\text{Fe}_2\text{O}_3 \cdot x\text{Bi}_2\text{O}_3$ as the egg white, and the outer mesoporous silica as the shell. The Fe and Bi bimetallic oxide active species are dispersed between the two silica layers. The HRTEM and STEM images indicate that the diameter of the Fe_3O_4 core is about 100 nm, and the thickness of the inner nonporous silica shell and the outer mesoporous silica shell are approximately 15 and 20 nm, respectively (Figs. S5(a)–S5(c) in the ESM). There are distinct boundaries between the two silica layers (Fig. S6 in the ESM), which allow the metallic oxides to be well dispersed on the surface of the inner nonporous silica to prevent aggregation.

The EDS mapping of the catalysts was consistent with the structures indicated by HRTEM and STEM (Figs. 1(c)–1(f) and S7–S9 in the ESM). The distribution of Si shows that the silica matrix is a double-layer hollow ball that is bigger than the solid Fe_3O_4 core. The whole Si sphere is a bit larger than the Bi sphere,

and the Bi sphere is as large as the gap sphere of the silica layers. This clearly presents that the $\text{Fe}_2\text{O}_3 \cdot x\text{Bi}_2\text{O}_3$ active component is sandwiched between the two layers of the silica shell.

No characteristic diffraction peaks related to Bi_2O_3 can be observed in the XRD patterns of the nanocomposites (Fig. S10 in the ESM), which suggests that the active species either existed in a highly dispersed amorphous state or in the pores of $\text{Fe}_3\text{O}_4@n\text{SiO}_2$ with sizes below 5 nm [67–68]; the TEM results support the later reason.

X-ray photoelectron spectroscopy analysis (Figs. 2(a)–2(c)) was performed to investigate the oxidation state of iron and bismuth bimetallic oxide nanoparticles encapsulated in the silicon. Two band energies at 724.9 and 711.5 eV are assigned to $\text{Fe } 2p_{1/2}$ and $\text{Fe } 2p_{3/2}$ of Fe^{3+} , respectively. The satellite peak at 719.5 eV is a major characteristic of Fe^{3+} in $\gamma\text{-Fe}_2\text{O}_3$ [69]. The peak positions of $\text{Bi } 4f_{7/2}$ and $\text{Bi } 4f_{5/2}$ appear at 159.9 and 165.1 eV and correspond to the presence of Bi_2O_3 [70–71].

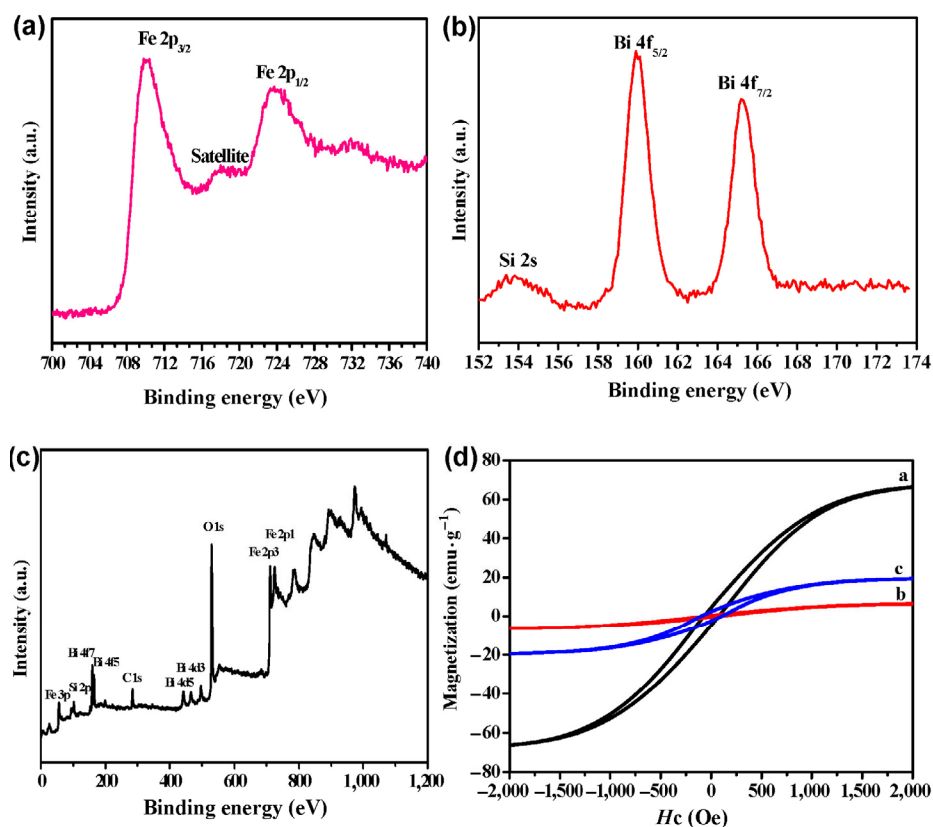


Figure 2 (a) XPS spectrum of Fe 2p region and (b) Bi 4f region. (c) XPS spectrum of SS-Fe-Bi. (d) Room-temperature hysteresis loops of (a) Fe_3O_4 , (b) $\text{Fe}_2\text{O}_3 \cdot x\text{Bi}_2\text{O}_3$, and (c) SS-Fe-Bi.

Furthermore, the surveyed spectrum indicates that the atomic concentrations of Fe and Bi are about 23.5% and 1.4%, respectively.

The magnetic properties of Fe_3O_4 , $\text{Fe}_2\text{O}_3 \cdot x\text{Bi}_2\text{O}_3$, and SS-Fe-Bi are shown in Fig. 2(d). The saturation magnetization (M_s) value of Fe_3O_4 is $71.9 \text{ emu} \cdot \text{g}^{-1}$, and that of $\text{Fe}_2\text{O}_3 \cdot x\text{Bi}_2\text{O}_3$ is $7.1 \text{ emu} \cdot \text{g}^{-1}$ at an applied field of 10,000 Oe. Considering the M_s values of magnetic Fe_3O_4 and the $\text{Fe}_2\text{O}_3 \cdot x\text{Bi}_2\text{O}_3$ nanoparticles, the catalyst active component, $\text{Fe}_2\text{O}_3 \cdot x\text{Bi}_2\text{O}_3$, is magnetically immobilized by the magnetic ferric oxide spheres. Furthermore, the M_s value of the SS-Fe-Bi catalyst is $21.2 \text{ emu} \cdot \text{g}^{-1}$, which is ascribed to coating of the silica spheres and the deposited weakly magnetic $\text{Fe}_2\text{O}_3 \cdot x\text{Bi}_2\text{O}_3$.

The optimal reactions were performed in a fixed-bed reactor that was filled with 650 mg of the well-developed catalyst. A solution of *p*-nitrophenol and $\text{N}_2\text{H}_4 \cdot \text{H}_2\text{O}$ in methanol was pumped through the heat catalyst cartridge under different conditions by an HPLC pump, and the product was analyzed with TLC and HPLC. The results are summarized in Table 2. The early investigations were performed using different concentrations of *p*-nitrophenol. The data in Table 2 indicate that *p*-nitrophenol (with a concentration below 0.8 M) can be completely converted to *p*-aminophenol with a 20% excess of stoichiometric hydrazine hydrate at 110 °C (entries 1–3) at a flow rate of $1 \text{ mL} \cdot \text{min}^{-1}$. A concentration of 0.5 M was chosen for further research based on the solubility of the other common reactants. We then reduce the amount of hydrazine hydrate because a perfect CTH reaction could provide a wonderful yield with a minimal excess of the hydrogen donor. The dosage of hydrazine was decreased to the stoichiometric amount, and the conversions with different flow rates were still acceptable (entries 4–5). A very small excess of hydrazine led to complete conversion (entry 6). Subsequently, the reaction temperature decreased from 110 to 80 °C, and all of the reactions still gave a full conversion with only a 7% excess of stoichiometric hydrazine hydrate (entries 6–8). When the flow rate of the mixture solution was increased to $2 \text{ mL} \cdot \text{min}^{-1}$ or even $3 \text{ mL} \cdot \text{min}^{-1}$, full conversions were obtained in every case (entries 9–10), which indicated that all of the nitrophenol was consumed in less than 20 s. Performing a catalyst-free

Table 2 Optimization of the reaction conditions for the reduction of 4-nitrophenol in a continuous-flow reactor using $\text{N}_2\text{H}_4 \cdot \text{H}_2\text{O}$ and SS-Fe-Bi^a

Entry	Conc. ($\text{mol} \cdot \text{L}^{-1}$)	$n(\text{N}_2\text{H}_4 \cdot \text{H}_2\text{O})$: $n(\text{p-nitrophenol})$	Temperature (°C)	Flow rate ($\text{mL} \cdot \text{min}^{-1}$)	Conversion (%)
1	0.2	1.8	110	1	>99
2	0.5	1.8	110	1	>99
3	0.8	1.8	110	1	>99
4	0.5	1.5	110	0.5	98
5	0.5	1.5	110	1	97
6	0.5	1.6	110	1	>99
7	0.5	1.6	100	1	>99
8	0.5	1.6	80	1	>99
9	0.5	1.6	80	2	>99
10	0.5	1.6	80	3	>99
11	0.5	1.6 (cat. free)	80	1	0

^aThe reactions were performed with 40 mmol of *p*-nitrophenol and hydrazine hydrate in 80 mL of methanol.

^bDetermined as the HPLC peak area percent.

reaction provided no consumption of the starting material (entry 11). These results reveal the superior activity of the SS-Fe-Bi catalyst.

One of the most significant characteristics of an immobilized catalyst is its extended usability. Therefore, we placed special emphasis on monitoring the SS-Fe-Bi catalyst for a prolonged time with the reduction of *p*-nitrophenol (0.5 M). The free volume of the catalyst cartridge was estimated, and every free volume of the reaction mixture that moved through the catalyst bed could be regarded as a cycle. Every 200 cycles, a 1.0 mL sample from the reaction mixture was collected and analyzed using HPLC during the continuous-flow experiment. Figure 3 shows that the catalyst could be used for more than 1,500 cycles at a flow rate of $1 \text{ mL} \cdot \text{min}^{-1}$ without any activity decline. This indicates the wonderful stability and long lifetime of the egg-like catalyst. The characterization of the catalyst after 1,500 cycles can be found in the supporting information (Figs. S5(d), S11, and S12 in the ESM). The excellent stability of the nanocatalyst may arise from the

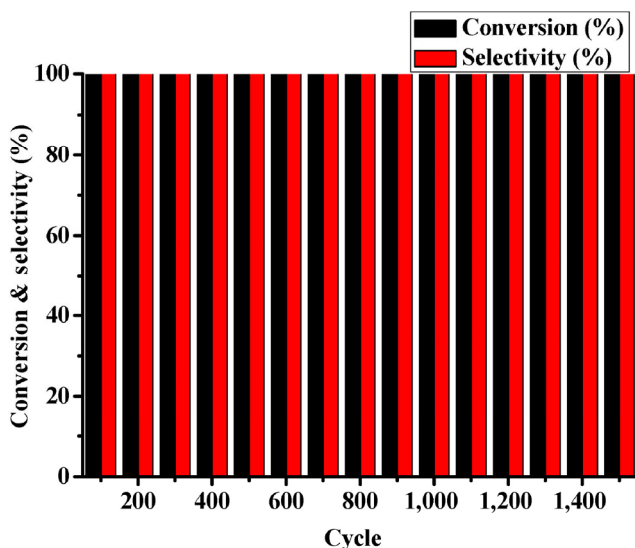


Figure 3 The long run test for the SS-Fe-Bi catalyst in a continuous-flow reactor for the reduction of *p*-nitrophenol.

following aspects: (1) The bimetallic oxide nanoparticles are magnetically immobilized, which may limit the unwanted change of crystallinity, which usually deactivates the catalyst. (2) The catalyst is further encapsulated by the microporous silicon shell, and the nanoparticles are well dispersed among the amino groups. These items prevent migration and coalescence of the catalyst during the catalytic reactions; thus, the catalyst maintains its initial activity for a long time.

According to this processing, the producing ability of the catalyst cartridge was up to $46 \text{ mmol} \cdot \text{g}^{-1} \cdot \text{h}^{-1}$. This indicates that the continuous reduction catalyzed by SS-Fe-Bi might be a practical approach for the synthesis of nitroarenes. Yet, the selectivity of the catalyst and the functionality tolerance of the catalytic protocol should be examined. We investigated the SS-Fe-Bi catalyzed reduction of structurally diverse nitro compounds in a fixed-bed continuous-flow reactor under optimized reaction conditions (Table 3). Full conversion was achieved for all substrates with an excellent yield to the anticipated anilines by this technology. The reactant solubility was a critical factor for the continuous-flow technique. Commonly, anilines are more soluble than nitroarenes in methanol because of molecular polarity; thus, the reaction concentration strongly depends on the solubility of the nitroarenes. The nitroarenes were dissolved in different concentrations of methanol based on their different

Table 3 Reduction of nitroarenes with $\text{N}_2\text{H}_4 \cdot \text{H}_2\text{O}$ and catalyzed by SS-Fe-Bi in a continuous-flow reactor^a

Entry	Substrate	Conc.Ar-NO ₂ (mol·L ⁻¹)	Product	Conversion ^c (%)	Selectivity ^d (%)
1		0.5		>99	100
2		1.0		>99	100
3		0.5		>99	100
4		0.25		>99	100
5		0.5		>99	100
6		0.5		>99	100
7 ^b		0.1		97	100
8		0.25		>99	100
9 ^b		0.3		95	100
10		0.5		>99	100
11		0.5		>99	100
12		0.5		>99	100
13		0.5		>99	100
14		0.1		>99	100
15		0.5		>99	100
16		0.2		93	100
17		0.1		>99	100
18		1.0		>99	100
19		0.25		>99	100
20 ^e		0.5		>99	100
21 ^e		0.5		>99	100

^aReaction performed using a $1.0 \text{ mL} \cdot \text{min}^{-1}$ flow rate of ArNO₂ and MeOH solutions with a 7% excess of $\text{N}_2\text{H}_4 \cdot \text{H}_2\text{O}$, with SS-Fe-Bi (650 mg) in a catalyst cartridge at 110 °C and 30 bar of backing pressure.

^bNaOH was used to make the substrates to become sodium salts, and the reaction solvent was MeOH + H₂O (MeOH:H₂O = 1:1).

^cDetermined as the HPLC peak area percent.

^dDetermined by GC-MS.

^eReduction of aliphatic nitro compounds.

solubilities. The easily soluble substrates, such as *p*-nitrotoluene can be easily reduced with a concentration of 1.0 M in a continuous-flow reactor (entry 2). Dehalogenation was usually observed in the catalytic hydrogenation; therefore, we used five chloro-nitroarenes to test the selectivity. Simple substrates, such as *p*-chloronitrobenzene and *o*-chloronitrobenzene, gave corresponding anilines in quantitative yields (entries 3–4), and this method also worked for multisubstituted substrates, such as 4-chloro-2-nitrophenol and 4-(4-chlorophenoxy) nitrobenzene (entries 5–6) with good chemoselectivity. The steric hindrance did not appreciably affect the reaction yields. Furthermore, 2,6-dichloro-4-nitrophenol was selectively reduced smoothly to generate the 2,6-dichloro-4-aminophenol, which was a significant intermediate for synthesis of chlorfluazuron and hexaflumuron, which are highly efficient and low residual pesticides. Furthermore, dehalogenation was successfully avoided under the reaction conditions for all compounds. This catalyst system was also selective for other functionalized nitroarenes, including the derivatives that contained alcohol, acid, ester, ether, amide, or amino groups. All of them were fully converted into the corresponding anilines without any functionality changes (entries 8–14). In particular, *p*-nitrobenzoic acid, which was a highly challenging example for the reduction of the nitro group because of the strong electron-withdrawing property of the free carboxylic acid group [72], was successfully reduced to the corresponding aniline with nearly full conversion. The reduction of 2,4-dinitrophenol gave 2-amino-4-nitrophenol as a single product with a nearly quantitative yield, which usually provided a complex mixture in the typical batch reduction (entry 16). Remarkably, some substrates bearing heterocyclic ring moieties (entries 17–19) were also charged to investigate the scope of our catalytic system. They were smoothly converted into corresponding anilines with satisfactory yields, while the heterocyclic rings remained intact. The small molecular nitroalkanes were smoothly converted into their corresponding aminoalkanes (entries 20, 21). In all cases, the azoxy, azo, and hydrazo compounds that were usually generated as the by-products in the reduction of nitroarenes were not detected in this reaction system.

The continuous-flow reaction system described above is superior to most other reported protocols. The good catalytic activity lets the reaction run at a low temperature, which is important in industrial procedures because the low reaction temperature produces useful anilines. The higher reaction temperature causes a faster reaction rate; however, we obtained a black product if the reduction of *p*-nitrophenol was performed at an extremely high temperature (i.e., above 120 °C). Furthermore, one catalyst cartridge was usually used for one kind of substrate in a continuous-flow microreactor. A used catalyst cartridge could not work for another reactant because the residues of the former product could not be entirely removed; thus, the later product would usually be impure unless the catalyst bed had been washed with a large amount of solvent, which would cause leaching of active components. However, all of the nitroarenes in Table 3 were reduced using the same catalyst cartridge. This occurred because the egg-like nanocatalyst is both stable and uniform. When the recycled catalyst cartridge was utilized to reduce another substrate, washing with a small amount of methanol (about 50 mL) could completely clean the catalyst bed. With this unique advantage, the continuous-flow reduction catalyzed by the egg-like catalyst is expected to be an ideal protocol for the synthesis of fine chemicals that are usually produced on a small scale.

Based on the reported literature [73] and the experimental results, a plausible reaction mechanism is proposed (Fig. 4). During this reaction process, the nitroaromatics and $N_2H_4 \cdot H_2O$ first diffuse through the mesoporous silica channel, and are then adsorbed on the surface of $Fe_2O_3 \cdot xBi_2O_3$. N_2H_4 sequentially loses electrons to generate N_2 and active H species (that inevitably combine to H_2 as a side reaction of hydrazine). The Fe^{3+} in $Fe_2O_3 \cdot xBi_2O_3$ converts to Fe^{2+} , and forms the catalytic cycle together with the oxidation of Fe^{2+} to Fe^{3+} by the group. The active H species and electro transfer to the adsorbed nitroarene, then the nitro compound gradually reduced to the aniline. The overall mechanism has been identified as: $Ar-NO_2 \rightarrow Ar-NOOH \rightarrow Ar-N(OH)_2 \rightarrow Ar-NOH \rightarrow Ar-NHOH \rightarrow Ar-NH \rightarrow Ar-NH_2$. The synergistic effect between the iron and bismuth oxides enhances the

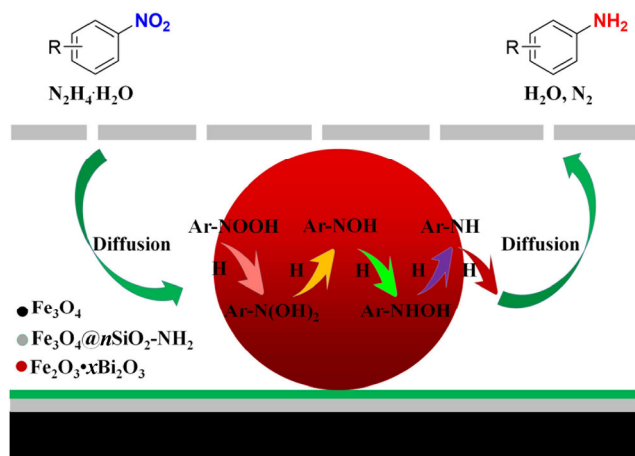


Figure 4 Possible mechanisms for catalytic reduction of aromatic nitro compounds with the catalyst SS-Fe-Bi.

stability of active H, so the utilization of N_2H_4 reached 98% in a stoichiometric reaction (Table 2, entry 4), and only a slight excess of hydrazine is required for the full conversion of the nitroaromatics.

4 Conclusions

In summary, a novel mesoporous-silica-protected egg-like SS-Fe-Bi nanocatalyst was synthesized using coprecipitation and a surface-protected etching method. This heterogeneous catalyst showed a high efficiency and excellent chemoselectivity for the reduction of various functionalized nitroarenes to corresponding anilines with a 7% stoichiometric excess of hydrazine hydrate. The catalytic reactions were performed in a fixed-bed continuous-flow reactor under relatively mild conditions with a nearly workup-free procedure. The reaction time could be less than 1 min with full conversion in all cases, and the catalyst cartridge could be reused and switched between different substrates. In the successful long run reduction of *p*-nitrophenol, 650 mg of the catalyst provided a productivity of 0.5 mmol every cycle for more than 1,500 cycles under the carefully optimized conditions. These indicated the excellent activity, perfect chemoselectivity, and outstanding lifetime of the catalyst. These advantages arise from the special structure: The presence of bismuth enhances the activity of iron oxide based catalyst, the active component $Fe_2O_3 \cdot xBi_2O_3$ is magnetically immobilized to the magnetic silica sphere, and it is further protected by the mesoporous silica shell

that suppresses the loss and aggregation of the nanocatalyst. This catalyst and the continuous protocol are expected to be used for the synthesis of fine chemicals.

Acknowledgements

This work was financially supported by National Natural Science Foundation of China (Nos. 21235004 and 21175080) and the Ministry of Science and Technology (No. 2013ZX09507005).

Electronic Supplementary Material: Supplementary material (HRTEM, STEM, EDS, 1H -NMR, ^{13}C -NMR, and GC-MS, characterization of catalyst and product) is available in the online version of this article at <https://doi.org/10.1007/s12274-017-1631-2>.

References

- [1] Hartman, R. L.; McMullen, J. P.; Jensen, K. F. Deciding whether to go with the flow: Evaluating the merits of flow reactors for synthesis. *Angew. Chem., Int. Ed.* **2011**, *50*, 7502–7519.
- [2] Pastre, J. C.; Browne, D. L.; Ley, S. V. Flow chemistry syntheses of natural products. *Chem. Soc. Rev.* **2013**, *42*, 8849–8869.
- [3] Porta, R.; Benaglia, M.; Puglisi, A. Flow chemistry: Recent developments in the synthesis of pharmaceutical products. *Org. Process Res. Dev.* **2016**, *20*, 2–25.
- [4] Wiles, C.; Watts, P. Continuous flow reactors: A perspective. *Green Chem.* **2012**, *14*, 38–54.
- [5] Gemoets, H. P. L.; Su, Y. H.; Shang, M. J.; Hessel, V.; Luque, R.; Noël, T. Liquid phase oxidation chemistry in continuous-flow microreactors. *Chem. Soc. Rev.* **2016**, *45*, 83–117.
- [6] Adamo, A.; Beingessner, R. L.; Behnam, M.; Chen, J.; Jamison, T.F.; Jensen, K. F.; Monbaliu, J. C. M.; Myerson, A. S.; Revalor, E. M.; Snead, D. R. et al. On-demand continuous-flow production of pharmaceuticals in a compact, reconfigurable system. *Science* **2016**, *352*, 61–67.
- [7] Tsubogo, T.; Oyamada, H. S.; Kobayashi, S. Multistep continuous-flow synthesis of (*R*)- and (*S*)-rolipram using heterogeneous catalysts. *Nature* **2015**, *520*, 329–332.
- [8] Gutmann, B.; Cantillo, D.; Kappe, C. O. Continuous-flow technology—a tool for the safe manufacturing of active pharmaceutical ingredients. *Angew. Chem., Int. Ed.* **2015**, *54*, 6688–6728.

- [9] He, Z.; Jamison, T. F. Continuous-flow synthesis of functionalized phenols by aerobic oxidation of grignard reagents. *Angew. Chem., Int. Ed.* **2014**, *53*, 3353–3357.
- [10] Cantillo, D.; Kappe, C. O. Immobilized transition metals as catalysts for cross-couplings in continuous flow—A critical assessment of the reaction mechanism and metal leaching. *ChemCatChem* **2014**, *6*, 3286–3305.
- [11] Irfan, M.; Glasnov, T. N.; Kappe, C. O. Heterogeneous catalytic hydrogenation reactions in continuous-flow reactors. *ChemSusChem* **2011**, *4*, 300–316.
- [12] Liu, X. Y.; Ünal, B.; Jensen, K. F. Heterogeneous catalysis with continuous flow microreactors. *Catal. Sci. Technol.* **2012**, *2*, 2134–2138.
- [13] Pascanu, V.; Hansen, P. R.; Gómez, A. B.; Ayats, C.; Platero-Prats, A. E.; Johansson, M. J.; Pericàs, M. A.; Martín-Matute, B. Highly functionalized biaryls via suzuki-miyaura cross-coupling catalyzed by Pd@MOF under batch and continuous flow regimes. *ChemSusChem* **2015**, *8*, 123–130.
- [14] Wiles, C.; Watts, P. Continuous process technology: A tool for sustainable production. *Green Chem.* **2014**, *16*, 55–62.
- [15] White, R. J.; Luque, R.; Budarin, V. L.; Clark, J. H.; Macquarrie, D. J. Supported metal nanoparticles on porous materials. Methods and applications. *Chem. Soc. Rev.* **2009**, *38*, 481–494.
- [16] Zhong, C. J.; Maye, M. M. Core-shell assembled nanoparticles as catalysts. *Adv. Mater.* **2001**, *13*, 1507–1511.
- [17] Kim, J.; Kim, H. S.; Lee, N.; Kim, T.; Kim, H.; Yu, T.; Song, I. C.; Moon, W. K.; Hyeon, T. Multifunctional uniform nanoparticles composed of a magnetite nanocrystal core and a mesoporous silica shell for magnetic resonance and fluorescence imaging and for drug delivery. *Angew. Chem., Int. Ed.* **2008**, *47*, 8438–8441.
- [18] Gai, S. L.; Yang, P. P.; Li, C. X.; Wang, W. X.; Dai, Y. L.; Niu, N.; Lin, J. Synthesis of magnetic, up-conversion luminescent, and mesoporous core-shell-structured nanocomposites as drug carriers. *Adv. Funct. Mater.* **2010**, *20*, 1166–1172.
- [19] Slowing, I. I.; Vivero-Escoto, J. L.; Trewyn, B. G.; Lin, V. S. Y. Mesoporous silica nanoparticles: Structural design and applications. *J. Mater. Chem.* **2010**, *20*, 7924–7937.
- [20] Stoeva, S. I.; Huo, F. W.; Lee, J. S.; Mirkin, C. A. three-layer composite magnetic nanoparticle probes for DNA. *J. Am. Chem. Soc.* **2005**, *127*, 15362–15363.
- [21] Deng, Y. H.; Deng, C. H.; Qi, D. W.; Liu, C.; Liu, J.; Zhang, X. M.; Zhao, D. Y. Synthesis of core/shell colloidal magnetic zeolite microspheres for the immobilization of trypsin. *Adv. Mater.* **2009**, *21*, 1377–1382.
- [22] Suteewong, T.; Sai, H.; Hovden, R.; Muller, D.; Bradbury, M. S.; Gruner, S. M.; Wiesner, U. Multicompartment mesoporous silica nanoparticles with branched shapes: An epitaxial growth mechanism. *Science* **2013**, *340*, 337–341.
- [23] Gawande, M. B.; Monga, Y.; Zboril, R.; Sharma, R. K. Silica-decorated magnetic nanocomposites for catalytic applications. *Coordin. Chem. Rev.* **2015**, *288*, 118–143.
- [24] Wang, C.; Chen, J. C.; Zhou, X. R.; Li, W.; Liu, Y.; Yue, Q.; Xue, Z. T.; Li, Y. H.; Elzatahry, A. A.; Deng, Y. H.; Zhao, D. Y. Magnetic yolk-shell structured anatase-based microspheres loaded with Au nanoparticles for heterogeneous catalysis. *Nano Res.* **2015**, *8*, 238–245.
- [25] Lu, A. H.; Salabas, E. L.; Schüth, F. Magnetic nanoparticles: Synthesis, protection, functionalization, and application. *Angew. Chem., Int. Ed.* **2007**, *46*, 1222–1244.
- [26] Deng, Y. H.; Qi, D. W.; Deng, C. H.; Zhang, X. M.; Zhao, D. Y. Superparamagnetic high-magnetization microspheres with an Fe₃O₄@SiO₂ core and perpendicularly aligned mesoporous SiO₂ shell for removal of microcystins. *J. Am. Chem. Soc.* **2008**, *130*, 28–29.
- [27] Liang, X. L.; Li, J.; Joo, J. B.; Gutiérrez, A.; Tillekaratne, A.; Lee, I.; Yin, Y. D.; Zaera, F. Diffusion through the shells of yolk-shell and core-shell nanostructures in the liquid phase. *Angew. Chem., Int. Ed.* **2012**, *51*, 8034–8036.
- [28] Astruc, D.; Lu, F.; Aranzas, J. R. Nanoparticles as recyclable catalysts: The frontier between homogeneous and heterogeneous catalysis. *Angew. Chem., Int. Ed.* **2005**, *44*, 7852–7872.
- [29] Gawande, M. B.; Goswami, A.; Asefa, T.; Guo, H. Z.; Biradar, A. V.; Peng, D. L.; Zboril, R.; Varma, R. S. Core-shell nanoparticles: Synthesis and applications in catalysis and electrocatalysis. *Chem. Soc. Rev.* **2015**, *44*, 7540–7590.
- [30] Lee, I.; Zhang, Q.; Ge, J. P.; Yin, Y. D.; Zaera, F. Encapsulation of supported Pt nanoparticles with mesoporous silica for increased catalyst stability. *Nano Res.* **2011**, *4*, 115–123.
- [31] Hu, H. W.; Xin, J. H.; Hu, H.; Wang, X. W.; Miao, D. G.; Liu, Y. Synthesis and stabilization of metal nanocatalysts for reduction reactions—A review. *J. Mater. Chem.* **2015**, *3*, 11157–11182.
- [32] El-Toni, A. M.; Habila, M. A.; Labis, J. P.; AlOthman, Z. A.; Alhoshan, M.; Elzatahry, A. A.; Zhang, F. Design, synthesis and applications of core-shell, hollow core, and nanorattle multifunctional nanostructures. *Nanoscale* **2016**, *8*, 2510–2531.
- [33] Jagadeesh, R. V.; Surkus, A. E.; Junge, H.; Pohl, M. M.; Radnik, J.; Rabeah, J.; Huan, H.; Schünemann, V.; Brückner, A.; Beller, M. Nanoscale Fe₂O₃-based catalysts for selective hydrogenation of nitroarenes to anilines. *Science* **2013**, *342*, 1073–1076.

- [34] Westerhaus, F. A.; Jagadeesh, R. V.; Wienhöfer, G.; Pohl, M. M.; Radnik, J.; Surkus, A. E.; Rabeah, J.; Junge, K.; Junge, H.; Nielsen, M. et al. Heterogenized cobalt oxide catalysts for nitroarene reduction by pyrolysis of molecularly defined complexes. *Nat. Chem.* **2013**, *5*, 537–543.
- [35] Zhu, K. L.; Shaver, M. P.; Thomas, S. P. Chemoselective nitro reduction and hydroamination using a single iron catalyst. *Chem. Sci.* **2016**, *7*, 3031–3035.
- [36] Yang, B.; Zhang, Q. K.; Ma, X. Y.; Kang, J. Q.; Shi, J. M.; Tang, B. Preparation of a magnetically recoverable nanocatalyst via cobalt-doped Fe₃O₄ nanoparticles and its application in the hydrogenation of nitroarenes. *Nano Res.* **2016**, *9*, 1879–1890.
- [37] Oubenali, M.; Vanucci, G.; Machado, B.; Kacimi, M.; Ziyad, M.; Faria, J.; Raspolli-Galetti, A.; Serp, P. Hydrogenation of *p*-chloronitrobenzene over nanostructured-carbon-supported ruthenium catalysts. *ChemSusChem* **2011**, *4*, 950–956.
- [38] Aditya, T.; Pal, A.; Pal, T. Nitroarene reduction: A trusted model reaction to test nanoparticle catalysts. *Chem. Commun.* **2015**, *51*, 9410–9431.
- [39] Zhao, P. X.; Feng, X. W.; Huang, D. S.; Yang, G. Y.; Astruc, D. Basic concepts and recent advances in nitrophenol reduction by gold- and other transition metal nanoparticles. *Coordin. Chem. Rev.* **2015**, *287*, 114–136.
- [40] Yu, L.; Zhang, Q.; Li, S. S.; Huang, J.; Liu, Y. M.; He, H. Y.; Cao, Y. Gold-catalyzed reductive transformation of nitro compounds using formic acid: Mild, efficient, and versatile. *ChemSusChem* **2015**, *8*, 3029–3035.
- [41] Wu, Y. E.; Wang, D. S.; Zhou, G.; Yu, R.; Chen, C.; Li, Y. D. Sophisticated construction of Au islands on Pt–Ni: An ideal trimetallic nanoframe catalyst. *J. Am. Chem. Soc.* **2014**, *136*, 11594–11597.
- [42] Gawande, M. B.; Rathi, A. K.; Tucek, J.; Safarova, K.; Bundaleski, N.; Teodoro, O. M. N. D.; Kvitek, L.; Varma, R. S.; Zboril, R. Magnetic gold nanocatalyst (nanocatalyst–Au): Catalytic applications for the oxidative esterification and hydrogen transfer reactions. *Green Chem.* **2014**, *16*, 4137–4143.
- [43] Guo, H. F.; Yan, X. L.; Zhi, Y.; Li, Z. W.; Wu, C.; Zhao, C. L.; Wang, J.; Yu, Z. X.; Ding, Y.; He, W. et al. Nanostructuring gold wires as highly durable nanocatalysts for selective reduction of nitro compounds and azides with organosilanes. *Nano Res.* **2015**, *8*, 1365–1372.
- [44] Jia, W. G.; Zhang, H.; Zhang, T.; Xie, D.; Ling, S.; Sheng, E. H. Half-sandwich ruthenium complexes with Schiff-base ligands: Syntheses, characterization, and catalytic activities for the reduction of nitroarenes. *Organometallics* **2016**, *35*, 503–512.
- [45] Wang, Y.; Rong, Z. M.; Wang, Y.; Zhang, P.; Wang, Y.; Qu, J. P. Ruthenium nanoparticles loaded on multiwalled carbon nanotubes for liquid-phase hydrogenation of fine chemicals: An exploration of confinement effect. *J. Catal.* **2015**, *329*, 95–106.
- [46] Gu, J.; Zhang, Z. Y.; Hu, P.; Ding, L. P.; Xue, N. H.; Peng, L. M.; Guo, X. F.; Lin, M.; Ding, W. P. Platinum nanoparticles encapsulated in MFI zeolite crystals by a two-step dry gel conversion method as a highly selective hydrogenation catalyst. *ACS Catal.* **2015**, *5*, 6893–6901.
- [47] Li, Z.; Yu, R.; Huang, J. L.; Shi, Y. S.; Zhang, D. Y.; Zhong, X. Y.; Wang, D. S.; Wu, Y. E.; Li, Y. D. Platinum–nickel frame within metal-organic framework fabricated *in situ* for hydrogen enrichment and molecular sieving. *Nat. Commun.* **2015**, *6*, 8248.
- [48] Iihama, S.; Furukawa, S.; Komatsu, T. Efficient catalytic system for chemoselective hydrogenation of halonitrobenzene to haloaniline using PtZn intermetallic compound. *ACS Catal.* **2016**, *6*, 742–746.
- [49] Li, L. Y.; Zhou, C. S.; Zhao, H. X.; Wang, R. H. Spatial control of palladium nanoparticles in flexible click-based porous organic polymers for hydrogenation of olefins and nitrobenzene. *Nano Res.* **2015**, *8*, 709–721.
- [50] El-Hout, S. I.; El-Sheikh, S. M.; Hassan, H. M. A.; Harraz, F. A.; Ibrahim, I. A.; El-Sharkawy, E. A. A green chemical route for synthesis of graphene supported palladium nanoparticles: A highly active and recyclable catalyst for reduction of nitrobenzene. *Appl. Catal. A: Gen.* **2015**, *503*, 176–185.
- [51] Karimi, B.; Mansouri, F.; Vali, H. A highly water-dispersible/magnetically separable palladium catalyst: Selective transfer hydrogenation or direct reductive *N*-formylation of nitroarenes in water. *ChemPlusChem* **2015**, *80*, 1750–1759.
- [52] Gu, X. M.; Qi, W.; Xu, X. Z.; Sun, Z. H.; Zhang, L. Y.; Liu, W.; Pan, X. L.; Su, D. S. Covalently functionalized carbon nanotube supported Pd nanoparticles for catalytic reduction of 4-nitrophenol. *Nanoscale* **2014**, *6*, 6609–6616.
- [53] Jang, Y.; Kim, S.; Jun, S. W.; Kim, B. H.; Hwang, S.; Song, I. K.; Kim, B. M.; Hyeon, T. Simple one-pot synthesis of Rh–Fe₃O₄ heterodimer nanocrystals and their applications to a magnetically recyclable catalyst for efficient and selective reduction of nitroarenes and alkenes. *Chem. Commun.* **2011**, *47*, 3601–3603.
- [54] Ganji, S.; Enumula, S. S.; Marella, R. K.; Rao, K. S. R.; Burri, D. R. RhNPs/SBA-NH₂: A high-performance catalyst for aqueous phase reduction of nitroarenes to aminoarenes at room temperature. *Catal. Sci. Technol.* **2014**, *4*, 1813–1819.
- [55] Enthaler, S.; Junge, K.; Beller, M. Sustainable metal catalysis with iron: From rust to a rising star? *Angew. Chem., Int. Ed.* **2008**, *47*, 3317–3321.
- [56] Junge, K.; Wendt, B.; Shaikh, N.; Beller, M. Iron-catalyzed

- selective reduction of nitroarenes to anilines using organosilanes. *Chem. Commun.* **2010**, *46*, 1769–1771.
- [57] Jagadeesh, R.V.; Wienhöfer, G.; Westerhaus, F. A.; Surkus, A. E.; Pohl, M. M.; Junge, H.; Junge, K.; Beller, M. Efficient and highly selective iron-catalyzed reduction of nitroarenes. *Chem. Commun.* **2011**, *47*, 10972–10974.
- [58] Cantillo, D.; Baghbanzadeh, M.; Kappe, C. O. *In situ* generated iron oxide nanocrystals as efficient and selective catalysts for the reduction of nitroarenes using a continuous flow method. *Angew. Chem., Int. Ed.* **2012**, *51*, 10190–10193.
- [59] Dey, R.; Mukherjee, N.; Ahammed, S.; Ranu, B. C. Highly selective reduction of nitroarenes by iron(0) nanoparticles in water. *Chem. Commun.* **2012**, *48*, 7982–7984.
- [60] Zhang, Q.; Lee, I.; Joo, J. B.; Zaera, F.; Yin, Y. D. Core-shell nanostructured catalysts. *Acc. Chem. Res.* **2013**, *46*, 1816–1824.
- [61] Moghaddam, M. M.; Pieber, B.; Glasnov, T.; Kappe, C. O. Immobilized iron oxide nanoparticles as stable and reusable catalysts for hydrazine-mediated nitro reductions in continuous flow. *ChemSusChem* **2014**, *7*, 3122–3131.
- [62] Loos, P.; Alex, H.; Hassfeld, J.; Lovis, K.; Platzek, J.; Steinfeldt, N.; Hübner, S. Selective hydrogenation of halogenated nitroaromatics to haloanilines in batch and flow. *Org. Process Res. Dev.* **2016**, *20*, 452–464.
- [63] Rathi, A. K.; Gawande, M. B.; Ranc, V.; Pechousek, J.; Petr, M.; Cepe, K.; Varma, R. S.; Zboril, R. Continuous flow hydrogenation of nitroarenes, azides and alkenes using maghemite–Pd nanocomposites. *Catal. Sci. Technol.* **2016**, *6*, 152–160.
- [64] Zhao, W. R.; Gu, J. L.; Zhang, L. X.; Chen, H. R.; Shi, J. L. Fabrication of uniform magnetic nanocomposite spheres with a magnetic core/mesoporous silica shell structure. *J. Am. Chem. Soc.* **2005**, *127*, 8916–8917.
- [65] Ge, J. P.; Zhang, Q.; Zhang, T. R.; Yin, Y. D. Core–satellite nanocomposite catalysts protected by a porous silica shell: Controllable reactivity, high stability, and magnetic recyclability. *Angew. Chem., Int. Ed.* **2008**, *47*, 8924–8928.
- [66] Zhang, C. F.; Lu, J. M.; Li, M. R.; Wang, Y. H.; Zhang, Z.; Chen, H. J.; Wang, F. Transfer hydrogenation of nitroarenes with hydrazine at near-room temperature catalysed by a MoO₂ catalyst. *Green Chem.* **2016**, *18*, 2435–2442.
- [67] Feng, W. H.; Dong, H. X.; Niu, L. B.; Wen, X.; Huo, L.; Bai, G. Y. A novel Fe₃O₄@nSiO₂@NiPd–PVP@mSiO₂ multi-shell core-shell nanocomposite for cinnamic acid hydrogenation in water. *J. Mater. Chem. A* **2015**, *3*, 19807–19814.
- [68] Beswick, O.; Yuranov, I.; Alexander, D. T. L.; Kiwi-Minsker, L. Iron oxide nanoparticles supported on activated carbon fibers catalyze chemoselective reduction of nitroarenes under mild conditions. *Catal. Today* **2015**, *249*, 45–51.
- [69] Gu, X. M.; Sun, Z. H.; Wu, S. C.; Qi, W.; Wang, H. H.; Xu, X. Z.; Su, D. S. Surfactant-free hydrothermal synthesis of sub-10 nm γ -Fe₂O₃–polymer porous composites with high catalytic activity for reduction of nitroarenes. *Chem. Commun.* **2013**, *49*, 10088–10090.
- [70] Nie, R. F.; Liang, D.; Shen, L.; Gao, J.; Chen, P.; Hou, Z. Y. Selective oxidation of glycerol with oxygen in base-free solution over MWCNTs supported PtSb alloy nanoparticles. *Appl. Catal. B: Environ.* **2012**, *127*, 212–220.
- [71] Rauf, A.; Sher Shah, M. S. A.; Choi, G. H.; Humayoun, U. B.; Yoon, D. H.; Bae, J. W.; Park, J.; Kim, W. J.; Yoo, P. J. Facile Synthesis of hierarchically structured Bi₂S₃/Bi₂WO₆ photocatalysts for highly efficient reduction of Cr(VI). *ACS Sustainable Chem. Eng.* **2015**, *3*, 2847–2855.
- [72] Feng, J.; Handa, S.; Gallou, F.; Lipshutz, B. H. Safe and selective nitro group reductions catalyzed by sustainable and recyclable Fe/ppm Pd nanoparticles in water at room temperature. *Angew. Chem., Int. Ed.* **2016**, *55*, 8979–8983.
- [73] Sheng, T.; Qi, Y. J.; Lin, X.; Hu, P.; Sun, S. G.; Lin, W. F. Insights into the mechanism of nitrobenzene reduction to aniline over Pt catalyst and the significance of the adsorption of phenyl group on kinetics. *Chem. Eng. J.* **2016**, *293*, 337–344.